

Dipolar Bose gas in highly anharmonic traps

Francesco Ancilotto^{1,2} and Flavio Toigo^{1,2}

¹*Dipartimento di Fisica e Astronomia "Galileo Galilei" and CNISM,
Università di Padova, Via Marzolo 8, 35122 Padova, Italy*

²*CNR-IOM Democritos, via Bonomea, 265 - 34136 Trieste, Italy*

(Dated: May 19, 2018)

By means of mean-field theory, we have studied the structure and excitation spectrum of a purely dipolar Bose gas in pancake-shaped trap where the confinement in the x-y plane is provided by a highly anharmonic potential resulting in an almost uniform confinement in the plane. We show that the stable condensates is characterized by marked radially structured density profiles. The stability diagram is calculated by independently varying the strength of the interaction and the trap geometry. By computing the Bogoliubov excitation spectrum near the instability line we show that soft "angular" rotons are responsible for the collapse of the system. The free expansion of the cloud after the trap is released is also studied by means of time-dependent calculations, showing that a prolate, cigar-shaped condensate is dynamically stabilized during the expansion, which would otherwise collapse. Dipolar condensates rotating with sufficiently high angular velocity show the formation of multiply-quantized giant vortices, while the condensates acquire a ring-shaped form.

PACS numbers:

I. INTRODUCTION

In recent years, ultracold gases of dipolar particles (which include atoms with large magnetic moments and polar molecules) have attracted a great deal of interest because of their peculiar properties, which are due to the presence of the anisotropic, long-range dipole-dipole interaction in addition to the usual short-range correlation interaction.

A dipolar Bose Einstein Condensate (BEC) has been first realized with a gas of ⁵²Cr atoms [1], where the dipolar interaction energy between magnetic moments was about 15% of the short-range interaction energy as calculated on the basis of the scattering length. Dipolar systems made of polar molecules have been achieved as well [2]. Since then, purely dipolar condensate have been realized by tuning to zero the scattering length. The properties of dipolar BEC have been the subject of numerous experimental and theoretical studies, extensively reviewed in Ref.[3] and Ref.[4].

The long-range nature of the dipolar interaction together with its anisotropic character leads in these system to the appearance of a rich variety of phenomena, whose properties depend crucially upon the shape of the trapping potential and of the interaction strength [1, 4–10].

A purely dipolar Bose gas (i.e. one where no short-range correlation interaction among the atoms is present, or where the dipole-dipole interaction is much larger than the contact interaction) is always unstable in the spatially uniform case. This can be seen by recalling that in a completely polarized uniform condensate of density n_0 , where all dipoles (each of magnitude d) are parallel to each other, the dispersion law for elementary excitations as derived within the Bogoliubov theory, is given by [3]:

$$\epsilon(\mathbf{k}) = [E_k^2 + 2E_k n_0 C_{dd} (\cos^2 \theta_k - 1/3)]^{1/2} \quad (1)$$

where $E_k = \hbar^2 k^2 / 2M$ and θ_k is the angle between the excitation momentum \mathbf{k} and the common direction of the dipoles. C_{dd} is the dipole-dipole interaction strength, proportional to d^2 (see the following). The instability is clearly seen from the fact that at small k and $\cos^2 \theta_k < 1/3$ the excitations energies become imaginary.

In a completely polarized condensate confined by a cigar-shaped (prolate) trap elongated along the direction of dipoles alignment, the interaction will be mainly attractive and the condensate is unstable towards collapse, similarly to the case of a cold gas with attractive short-range interactions (negative s-wave scattering length). Conversely, in pancake-shaped (oblate) traps the tendency of the dipoles to align along the polarization axis in order to increase their attractive head-to-tail interaction is counteracted by the strong confinement in this direction, which favors instead configurations with atoms or molecules laying in a plane orthogonal to their dipole moments. This effect may make the dipolar interaction energy predominantly repulsive, leading to stabilization of the BEC when the trap is oblate enough.

Therefore the dipolar gas offers the possibility of modifying the effective atom-atom interaction by modifying the trap geometry, which can easily be controlled in experiments.

It has been shown [11] that pancake dipolar condensates may exhibit a roton-maxon feature in the excitation spectrum. The presence, position and depth of the roton minimum can be tuned by varying the density, the confining potential and the short-range interaction strength. Since the superfluid critical velocity, as obtained from the Landau's argument, is reduced in the presence of a roton minimum, this opens the possibility of manipulating the superfluid properties of trapped condensates.

When the roton gap disappears the condensate becomes intrinsically unstable: since the instability occurs at a specific value of the momentum, this points to the possibility of realizing a non-uniform ground-state. The

associated "self-assembled" density modulations, that are expected in the high density regime, can have a supersolid character[12]. In spite of this exciting possibility, no conclusive evidence has been gathered so far [13] that a supersolid phase of dipolar BEC actually exists.

A purely dipolar (i.e. the s-wave scattering length is $a = 0$) condensate in pancake-shaped traps is stable[14], provided the number of atoms/molecules is not too large. The stability diagram for dipolar condensates in pancake-like traps has been calculated in Ref.[9], by using the time-dependent Gross-Pitaevskii (GP) equation.

In a narrow region of the stability diagram, bi-concave shaped ("blood cell") condensate wavefunctions have been found[9, 15], with the maximum density away from the center of the cloud. Such effect is due to the long-range, mainly repulsive forces in oblate traps, in a way very much similar to the accumulation of charges on the surface of conducting materials. These peculiar structures are predicted to exist in a very narrow portion of the stability diagram, and also very close to the instability line. The soft-mode which is responsible for the collapse of these bi-concave condensates when the instability edge is reached is characterized by azimuthal density oscillations with angular momentum quantum number $m > 0$ ("angular" rotons), as opposed to the soft modes which drive the collapse of a "normal" condensate with isotropic interactions (where the maximum density is at the center), where $m = 0$ instead.

The observation of such bi-concave states is experimentally difficult because they have a small contrast (i.e. small density inhomogeneities), and moreover the region in the parameter space where they exist covers a very small area, very close to the instability line. The structure and dynamics of bi-concave dipolar condensates has been theoretically investigated using the GP equation near the threshold for instability, and a possible experimental signature of their appearance have been proposed in Ref.[16], in the form of non trivial angular distribution of the products of the system once the collapse is induced by varying the scattering length.

The superfluid character of dipolar condensate is signalled by the formation of quantized vortices in a rotating condensate. For this reason, the theoretical study of vortex states in dipolar systems has been pursued by several groups. In general, rotation of a harmonically trapped dipolar gas is found to affect the stability of the condensate[17–23]. Vortex states in dipolar systems in toroidal traps have been studied as well[24], where an azimuthal dependence of a particle density was found, characterized by symmetry-breaking density profiles where the density is inhomogeneously distributed along the torus.

The collapse dynamics of a ^{52}Cr dipolar condensate, induced by a sudden reduction of the s-wave scattering length characterizing the contact interaction below a threshold value, has been studied in Ref.[25, 26]. The collapse dynamics, triggered either by an adiabatic or nonadiabatic change in the ratio between the dipolar and

the contact interaction strength, has been theoretically studied in Ref.[26], where both "global" (i.e. characterized by highly elongated or flattened shapes of the atomic cloud) and "local" (i.e. characterized by inhomogeneous density profiles like shells, disks or stripes) regimes of collapse were observed.

A rather complex spatial pattern characterizes the dynamics of the cloud expansion and collapse reported in Ref.[25], involving an anisotropic, d-wave symmetric explosion of a spherical condensate. The collapse of pancake-shaped clouds has been studied in Ref.[27], showing similar qualitative behavior. The collapse dynamics as imaged during the experiment is quantitatively reproduced by numerical simulations based on the GP equation without any adjustable parameter[25]. The collapse of disc-shaped Bose dipolar gases has also been numerically studied in real-time dynamics in Ref.[28].

At variance with all the above investigations, where the confinement has always been chosen to be harmonic, even if anisotropic, in the following we will study a purely dipolar BEC confined by pancake-shaped trap potentials characterized by a tightly harmonic confinement along the z-direction (corresponding to the dipole polarization axis) but highly anharmonic in the x-y plane ("flat" confinement). This choice is suggested by the fact that in such a trap, easily implemented experimentally, the system motion in the x-y plane is almost unaffected by the trap details within the region of confinement, while the residual effect is due to the steep confinement at the system boundaries. The combination of these effects enhances the characteristic features associated with the non-local dipolar interaction with respect to the case of harmonic confinement. In fact we will show that, as a result of such confinement, highly structured densities of the dipolar BEC are obtained, generalizing the "blood cell" condensate shapes predicted for harmonic confinement. These highly structured radial density profiles might be easily observed experimentally since they are present in a wide portion of the stability diagram.

We use the GP equation to compute both static and dynamical properties of these systems. The validity of mean-field approximation was tested using many-body Monte Carlo methods[29, 30] and found to provide a correct description of the dipolar gas in the dilute limit $na^3 \ll 1$, i.e. at very low densities and/or away from shape resonances.

We will determine the stability diagrams of the dipolar condensate as both the strength parameter and the trap aspect ratio are varied, and show that the systems undergo collapse for sufficiently large coupling parameter and/or sufficiently large aspect ratios.

We find that the lowest excitation mode which becomes soft close to the instability has an azimuthal dependence proportional to $\sin(3\phi)$ and $\sin(4\phi)$: the condensate is thus expected to collapse with density modulations in the angular coordinates which break the cylindrical symmetry characterizing the ground-state structures.

We have also studied the behavior of the condensate

when subject to a rotation with a constant angular velocity Ω around an axis parallel to the polarization direction: for sufficiently high values of Ω the dipolar condensate develops multiple quantized vortices. Eventually, a single giant, multiply quantized vortex appears, while the condensate density acquires the shape of a narrow torus.

Finally, we have studied the free expansion of the "blood-cell" condensate after the confining trap is released and find that the expansion is characterized by an elongation into a cigar-shaped dipolar condensate that would otherwise be unstable towards collapse under stationary conditions. Such dynamical stabilization of a cigar-shaped, purely dipolar condensate should be easily imaged in experiments.

II. METHODS AND CALCULATIONS

We assume that all the N atoms (molecules) of the system are in a Bose-Einstein condensate described by the wavefunction $\Phi(\mathbf{r})$. The direction of dipole polarization is assumed to be along the z -axis. The energy of the system at the mean-field level is expressed by the functional

$$E = \int \left[\frac{\hbar^2}{2M} |\nabla \Phi(\mathbf{r})|^2 + V_t(\mathbf{r}) |\Phi(\mathbf{r})|^2 + \frac{g}{2} |\Phi(\mathbf{r})|^4 \right] d\mathbf{r} + \frac{1}{2} \int \int V_{dd}(|\mathbf{r} - \mathbf{r}'|) |\Phi(\mathbf{r})|^2 |\Phi(\mathbf{r}')|^2 d\mathbf{r} d\mathbf{r}' \quad (2)$$

The above functional includes a kinetic pressure term, a term describing the trap potential used to confine the system, the short-range ("contact") mean-field interaction energy, and the dipole-dipole interaction potential:

$$V_{dd}(\mathbf{R}) = \frac{C_{dd}}{4\pi} \frac{(1 - 3\cos^2\theta)}{R^3} \quad (3)$$

where $\mathbf{R} = \mathbf{r} - \mathbf{r}'$ and θ is the angle between the vector \mathbf{R} and the polarization direction z .

In the case of polar molecules the prefactor is d^2/ϵ_0 , where d is the electric dipole moment of the molecule and ϵ_0 is the permittivity of the vacuum. In the case of magnetic interaction the prefactor is instead $\mu_0\mu_d^2$, where μ_d is the magnetic dipole moment of each atom and μ_0 is the permeability of free space.

The minimization of the above energy functional leads to the following Euler-Lagrange equation

$$\hat{H}\Phi(\mathbf{r}) = \mu\Phi(\mathbf{r}) \quad (4)$$

where μ is a Lagrange multiplier whose value is determined by the normalization condition $\int |\Phi(\mathbf{r})|^2 d\mathbf{r} = N$, and

$$\hat{H} \equiv -\frac{\hbar^2}{2M} \nabla^2 + V_t(\mathbf{r}) + g|\Phi(\mathbf{r})|^2 + \frac{C_{dd}}{4\pi} \int \frac{(1 - 3\cos^2\theta)}{(|\mathbf{r} - \mathbf{r}'|)^3} |\Phi(\mathbf{r}')|^2 d\mathbf{r}' \quad (5)$$

We will consider in the following a purely dipolar condensate, i.e. we take from now on $g = 0$, implicitly assuming that the interparticle interaction is dominated by the dipole-dipole forces ($d^2 \gg |g| = 4\pi\hbar^2|a_s|/M$, where a_s is the s-wave scattering length).

We consider here the case where the trapping potential is highly anharmonic ("flat") in the x-y plane, and harmonically confined along the polarization direction z :

$$V_t(\mathbf{r}) = \frac{M}{2} \omega_z^2 z^2 + \kappa(x^2 + y^2)^{\gamma/2} \quad (6)$$

where $\gamma > 2$.

Highly anharmonic potentials can be realized in principle with the current laser optic techniques, as suggested by the theoretical calculations of Ref.[31]. The resulting trapping potential behaves as $V_t(\rho) \propto \rho^{2l}$, where $\rho = \sqrt{x^2 + y^2}$ is the radial distance from the beam center. Very flat confining potentials in the x-y plane are obtained for large values of l , although already for $l > 4$ the condensate is characterized by an almost constant density over the entire trap volume in the case of purely repulsive BEC[31]. The possibility of studying a spatially uniform quantum gas by loading the gas in a three-dimensional, quasi-uniform potential has also been demonstrated in Ref.[32]. The leading-order correction to the flatness of the box potential was found to be $\propto \rho^{13\pm 2}$, which is equivalent to a flat potential for most many-body studies.

In the following, we will take $\gamma = 10$ in the expression (6) for the trap potential.

Upon scaling lengths by $a_z \equiv \sqrt{\hbar/M\omega_z}$ and energies by $\hbar\omega_z$, and also by imposing that the dimensionless wavefunction is normalized to unity, i.e. $\Phi(\mathbf{r}) = \sqrt{N/a_z^3} \tilde{\Phi}(\tilde{\mathbf{r}})$ the equation (4) can be written in dimensionless form as:

$$\left[-\frac{\tilde{\nabla}^2}{2} + \frac{1}{2} \tilde{z}^2 + \left(\frac{a_z}{r_0}\right)^{\gamma+2} \frac{1}{2} (\tilde{x}^2 + \tilde{y}^2)^{\gamma/2} \right] \tilde{\Phi}(\tilde{\mathbf{r}}) + D \int \frac{(1 - 3\cos^2\theta)}{(|\tilde{\mathbf{r}} - \tilde{\mathbf{r}}'|)^3} |\tilde{\Phi}(\tilde{\mathbf{r}}')|^2 d\tilde{\mathbf{r}}' \tilde{\Phi}(\tilde{\mathbf{r}}) = \tilde{\mu} \tilde{\Phi}(\tilde{\mathbf{r}}) \quad (7)$$

Here $r_0 \equiv (\hbar^2/2M\kappa)^{1/(\gamma+2)}$ is the characteristic length for the anharmonic potential, expressed in terms of the parameter κ appearing in Eq.(6). From equation (7) it appears that two dimensionless parameters determine the solutions of the GP equation for a purely dipolar BEC in the trapping potential (6):

$$\lambda = \frac{a_z}{r_0} \quad D = NC_{dd}M/4\pi\hbar^2 a_z \quad (8)$$

λ controls the aspect ratio of the trap while D controls the dipole-dipole interaction strength.

This equation will be solved numerically, to yield the lowest energy state Φ describing the condensate in the

ground-state for a given pair λ, D . We do this by propagating it in imaginary time, i.e. by solving the equation

$$\frac{\partial \Phi}{\partial t} + (\hat{H} - \mu)\Phi(\mathbf{r}) = 0 \quad (9)$$

The wave function $\Phi(\mathbf{r})$ is represented on a three-dimensional uniform mesh in real space, with periodic boundary conditions imposed on the system. The cell must be wide enough to avoid spurious dipole-dipole interactions between the atomic clouds and its periodically repeated images[33]. The starting wavefunction is chosen in the form of a narrow gaussian placed in the center of the trap (although we verified that the final, minimum energy structure does not depend upon a particular choice for the initial wavefunction).

To compute the spatial derivatives appearing in the GP equation (4), we used an accurate 13-point finite-difference formula [34]. The convolution integral in the potential energy term of Eq.(7) is efficiently evaluated in reciprocal space by using Fast Fourier transform techniques, and by recalling that the Fourier transform of V_{dd} is[3]

$$\tilde{V}_{\mathbf{k}} = \frac{C_{dd}}{3}(3\cos^2\alpha - 1) \quad (10)$$

where α is the angle between \mathbf{k} and the z -axis.

In order to compute the excitation spectrum, we make the usual Bogoliubov transformation to a Hamiltonian describing a collection of non-interacting quasi-particles for which the condensate is the vacuum:

$$\Psi(\mathbf{r}, t) = e^{-i\mu t/\hbar}[\Phi(\mathbf{r}) + u(\mathbf{r})e^{-i\omega t} - v^*(\mathbf{r})e^{i\omega t}] \quad (11)$$

where $u(\mathbf{r})$ and $v(\mathbf{r})$ are the wavefunctions of the excitation mode and $\Phi(\mathbf{r})$ is the solution of Eq.(4).

The computation of the excited states is particularly demanding from a computational point of view if performed, as we did in the present work, in three-dimensional cartesian coordinates (an alternative approach, exploiting the cylindrical symmetry of the problem, has been developed in Ref.[33]). It is thus important, in order to reduce the computational burden, to use the smallest possible number of points in the spatial mesh that guarantee an accurate representation of the ground-state wavefunction Φ . By studying the convergence in energy of the solution with increasing number of points in the mesh, we verified that a relatively coarse grid with spacing $\Delta x \sim 0.3a_z$ is enough to accurately describe $\Phi(\mathbf{r})$.

Because of our use of Fourier Transform techniques, which imply that periodic boundary conditions must be imposed in our calculations, we can expand the wavefunction Φ and the complex functions u, v in the form

appropriate to a periodic system:

$$\Phi(\mathbf{r}) = \sum_{\mathbf{G}} \Phi_{\mathbf{G}} e^{i\mathbf{G} \cdot \mathbf{r}} \quad (12)$$

$$u(\mathbf{r}) = \sum_{\mathbf{G}} u_{\mathbf{G}} e^{i\mathbf{G} \cdot \mathbf{r}} \quad (13)$$

$$v(\mathbf{r}) = \sum_{\mathbf{G}} v_{\mathbf{G}} e^{i\mathbf{G} \cdot \mathbf{r}} \quad (14)$$

In the above expansions, the \mathbf{G} -vectors are the reciprocal lattice vectors appropriate to the space symmetry of the simulation cell containing the dipolar cloud. In the present case, a simple orthorhombic geometry is used, with a computational cell of sides $L_x = L_y$ and L_z . Substituting the expressions (14) into the time-dependent GP equation $[i\hbar\partial/\partial t - \hat{H}]\Psi(\mathbf{r}, t) = 0$ associated with the Hamiltonian (5), and keeping only terms linear in the functions u, v , one obtains a set of equations for the coefficients $\{u_{\mathbf{G}}\}$ and $\{v_{\mathbf{G}}\}$ that can be recasted into the following matrix form [35]:

$$\begin{bmatrix} \mathbf{A} & \mathbf{B} \\ -\mathbf{B} & -\mathbf{A} \end{bmatrix} \begin{pmatrix} \mathbf{u} \\ \mathbf{v} \end{pmatrix} = \hbar\omega \begin{pmatrix} \mathbf{u} \\ \mathbf{v} \end{pmatrix} \quad (15)$$

where the matrices (with dimensions $(n_r^3 \times n_r^3)$, where n_r is the real space mesh used to integrate the stationary GP equation) are defined as:

$$\mathbf{A}_{\mathbf{G}, \mathbf{G}'} \equiv \delta_{\mathbf{G}, \mathbf{G}'} \left[\frac{\hbar^2 \mathbf{G}^2}{2M} - \mu \right] + \tilde{U}_{\mathbf{G}-\mathbf{G}'} + \sum_{\mathbf{G}''} \Phi_{\mathbf{G}''-\mathbf{G}'} \Phi_{\mathbf{G}-\mathbf{G}''} \tilde{V}_{\mathbf{G}''} \quad (16)$$

$$\mathbf{B}_{\mathbf{G}, \mathbf{G}'} \equiv - \sum_{\mathbf{G}''} \Phi_{\mathbf{G}''-\mathbf{G}'} \Phi_{\mathbf{G}-\mathbf{G}''} \tilde{V}_{\mathbf{G}''} \quad (17)$$

The quantities $\tilde{U}_{\mathbf{G}}$ in Eqns.(16) are defined through

$$V_t(\mathbf{r}) + \int V_{dd}(|\mathbf{r} - \mathbf{r}'|) |\Phi(\mathbf{r}')|^2 d\mathbf{r}' = \sum_{\mathbf{G}} \tilde{U}_{\mathbf{G}} e^{i\mathbf{G} \cdot \mathbf{r}} \quad (18)$$

The excitation frequencies $\omega(\mathbf{k})$ can be determined from the solutions of the above non-Hermitian eigenvalue problem. This can be reduced to a non-Hermitian problem of *half* the dimension (thus largely reducing the computational cost of diagonalization) by means of a unitary transformation [36]:

$$(\mathbf{A} - \mathbf{B})(\mathbf{A} + \mathbf{B})|\mathbf{u} + \mathbf{v}\rangle = (\hbar\omega)^2 |\mathbf{u} + \mathbf{v}\rangle \quad (19)$$

If needed, one may calculate the separate \mathbf{u}, \mathbf{v} by properly combining the eigenvectors of Eq. (19) with those of the associated eigenvalue problem

$$(\mathbf{A} + \mathbf{B})(\mathbf{A} - \mathbf{B})|\mathbf{u} - \mathbf{v}\rangle = (\hbar\omega)^2 |\mathbf{u} - \mathbf{v}\rangle, \quad (20)$$

again of reduced dimensions.

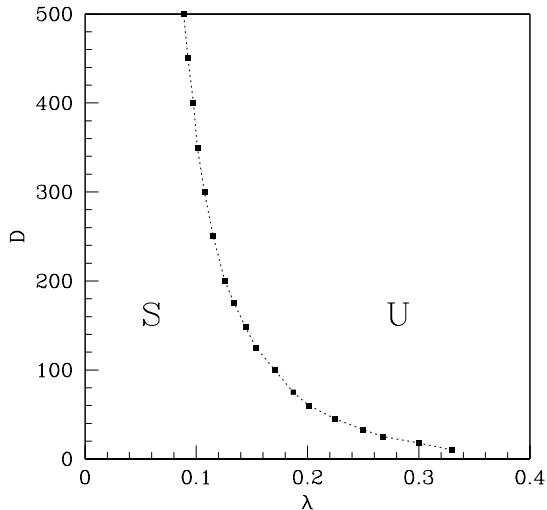


FIG. 1: Calculated stability diagram in the $D - \lambda$ plane.

III. RESULTS AND DISCUSSION

We have solved the stationary GP equation in imaginary time, as described in the previous Section, for different pairs of values (λ, D) : possible outcome of the calculations are either stable, converged states or "collapsed" states where during the evolution in imaginary time the density of the system catastrophically shrinks within a narrow spatial region.

The resulting stability diagram is shown in Fig.1, where a line in the $D - \lambda$ plane separates the stable (S) configurations from the unstable (U) ones. It appears that higher values of D (strong dipole-dipole coupling or large number of particles) and/or larger values of the aspect ratio λ (weaker confinement in the z -direction) make the system unstable towards collapse.

The density profiles associated with the condensate structures in the stable part of Fig.(1) are characterized by marked radial inhomogeneities, and differ considerably from the usual appearance of harmonically trapped dipolar gas clouds, where the maximum density is usually in the center of the trap. We show in Fig.2 several structures obtained for different pairs (λ, D) . Here the number density n is defined as $n(\mathbf{r}) = |\tilde{\Phi}(\mathbf{r})|^2$. Common to these structure is the accumulation towards the trap periphery, due to the interaction between dipoles, which results in a dense circular edge. Additional secondary peaks may appear for different values of (λ, D) . One may recognize in panel (c) a bi-concave ("blood cell") structure like the ones discussed in the previous Section, but with a much

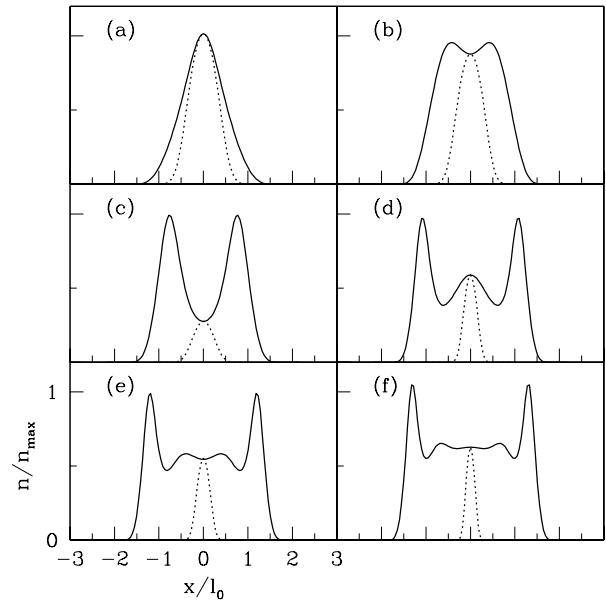


FIG. 2: Density profiles (normalized to the maximum density value) of stable configurations, shown along a cut in the x - y plane across the trap center, for different values of D and λ . (a): $D = 10$, $\lambda = 0.28$; (b): $D = 25$, $\lambda = 0.24$; (c): $D = 50$, $\lambda = 0.20$; (d): $D = 150$, $\lambda = 0.13$; (e): $D = 250$, $\lambda = 0.1$; (f): $D = 400$, $\lambda = 0.08$. The dotted lines show the density profile along the z -direction.

higher contrast than those realizable in harmonic traps. Multiple radial peaks appear as well for different trap geometries and/or strength parameter values.

In Fig.3 the ground state density profile of the bi-concave condensate shown in panel (c) of Fig.(2) is shown using equal density color maps in the x - y and x - z planes, respectively.

Unlike the case of harmonic confinement in the x - y plane, where concave structures with maximum density away from the trap center appears only in very small portion of the stability diagram, in the present case such shapes are easily realized with a variety of (λ, D) pairs spanning a large portion of the stability region in the diagram of Fig.(1). As an example, we show in Fig.(4) and Fig.(5) the ground-state density profiles for different choices of (λ, D) . Fig.(4) shows the structures associated to a fixed value of D and different values of λ . It appears that lower values of λ (i.e. corresponding to a tighter confinement of the dipolar gas along the z -direction) result in less structured clouds. Fig.(??) shows instead the structures associated with a fixed value of λ and different values of the interaction parameter D . Less structured clouds now correspond to lower values of D .

Collective modes of dipolar condensates under harmonic confinement have been analyzed in Ref.[9] (see also

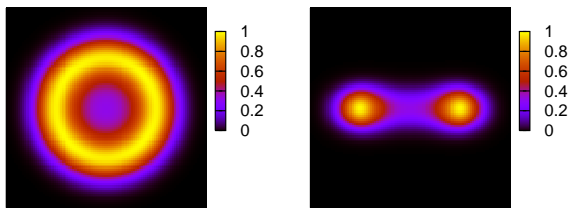


FIG. 3: (color online) Equal-density map (shown in the x-y and x-z plane, respectively) for the condensate with $D=50$ and $\lambda = 0.20$.

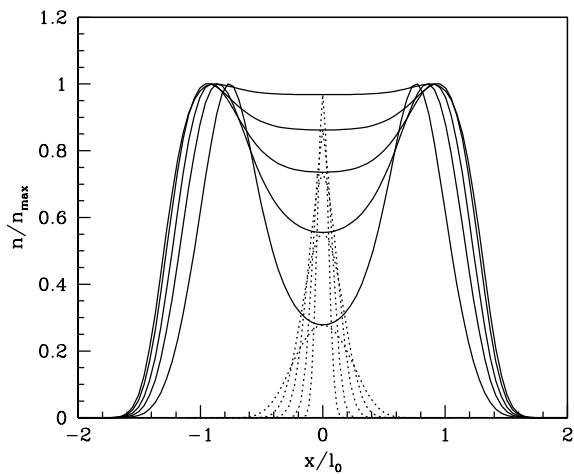


FIG. 4: Density profiles (normalized to the maximum density value) shown along the x-direction, for $D = 50$ and $\lambda = 0.06, 0.10, 0.14, 0.18, 0.20$. Approaching the instability line with higher values of λ correspond to more concave structures. The dotted lines show the density profile along the z-direction.

Ref.[4]). As discussed in the Introduction, two possible solution of the stationary GP equation have been found: a pancake shaped condensate (with the maximum of the density at the trap center) or a bi-concave shaped condensate which appears in a narrow region of the stability region. In the pancake case, the mode that drives the instability is a "radial" roton, i.e. it has a radial nodal pat-

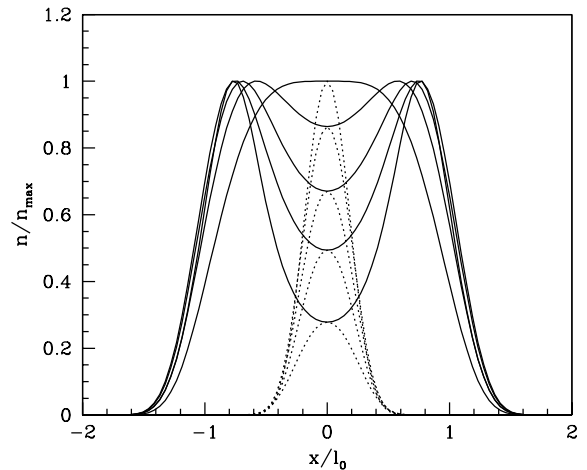


FIG. 5: Density profiles (normalized to the maximum density value) shown along the x-direction, for $\lambda = 0.20$ and $D = 10, 20, 30, 40, 50$. Approaching the instability line with higher values of D correspond to more concave structures. The dotted lines show the density profile along the z-direction.

tern ($m = 0$ projection of the angular momentum on the z-axis). In a bi-concave condensate the mode going soft exhibits density modulations along the ring corresponding to non-zero m ("angular" roton), with a subsequent breaking of the cylindrical symmetry[9].

For completeness, by using the Bogoliubov-deGennes equation formalism discussed in the previous Section, we have also computed the excitation spectrum of selected structures as a function of D for a given value of λ , starting below the stability line of Fig.(1) and increasing D , until the instability line is reached.

The resulting excitation frequencies for the case $\lambda = 0.2$ are shown in Fig.(6), where the calculated frequencies ω are shown as a function of D . By approaching the instability value it appears that several modes become soft. In particular, two modes (those originating at $\omega = 0.5\omega_z$ and $\omega = 0.34\omega_z$ for $D = 0$) have frequencies that go to zero right at the edge of collapse.

The local density fluctuations associated with these excitation modes can be calculated from

$$\Delta n(\mathbf{r}) = |u(\mathbf{r}) - v(\mathbf{r})|^2 \quad (21)$$

The density fluctuations $\Delta n(\mathbf{r})$ (shown with a map of equal density colors in the x-y plane) for the two soft

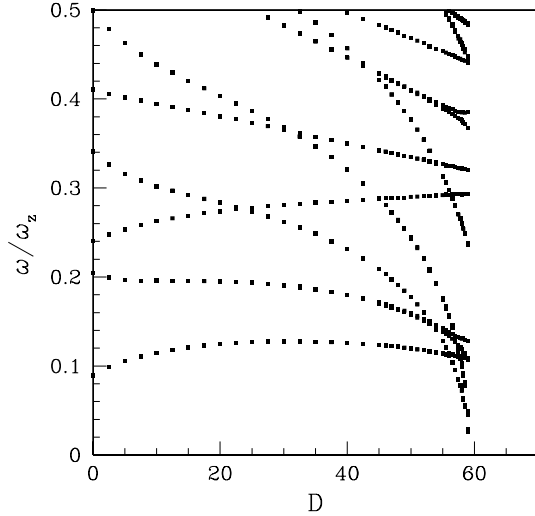


FIG. 6: Excitation spectrum for dipolar condensates with $\lambda = 0.2$, as a function of the strength parameter D .

modes which drive the collapse of the cloud are shown in Fig.(7).

From Fig.(7) it appears that such modes have an azimuthal dependence proportional to $\sin(3\phi)$ and $\sin(4\phi)$: the condensate is thus expected to collapse with density modulations in the angular coordinates which breaks the cylindrical symmetry. A similar breaking pattern has also been observed in the collapse of harmonically trapped Bose clouds in pancake-shaped condensates from numerical simulations based on the GP equation[28].

We have also studied the character of the soft mode responsible for the collapse of "normal" condensate clouds (i.e. with the maximum of the density at the center of the trap). One such configuration is shown in panel (a) of Fig.(2). In this case we find that the mode that drives the instability has a radial nodal pattern ($m = 0$ projection of the angular momentum on the z-axis), similarly to what is found for harmonically trapped condensates[4, 9].

Next, we studied how the dipolar condensate evolves dynamically after the trap is released. The time evolution is obtained by solving the time-dependent GP equation:

$$i\hbar \frac{\partial \Psi(\mathbf{r}, t)}{\partial t} = [\hat{H} - \frac{i\hbar L_3}{2} |\Psi|^4] \Psi(\mathbf{r}, t) \quad (22)$$

We have added to the dipolar GP hamiltonian a dissipative term proportional to $L_3 \sim 2 \times 10^{-40} \text{ m}^6 \text{ s}^{-1}$ which describes three-body losses[25].

We have used the Runge-Kutta-Gill fourth-order method [37] to propagate in time the solutions of the pre-

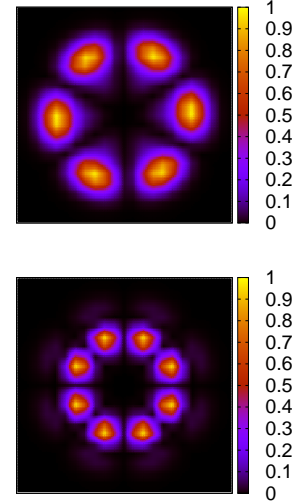


FIG. 7: (color online) Number density fluctuations associated with the two soft modes shown in Fig.(6).

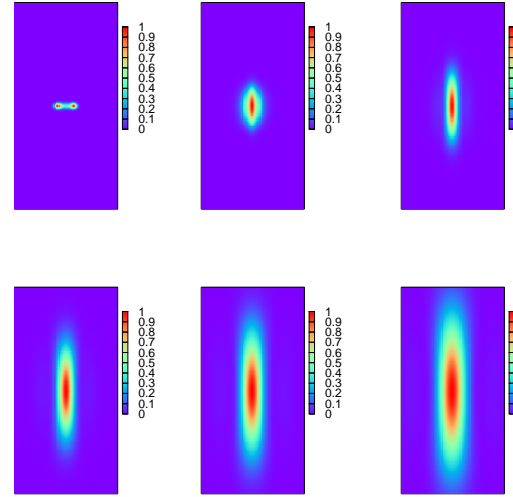


FIG. 8: (color online) Time evolution of the condensate after the release of the trap. From left to right and top to bottom, the time instants are: $t = 0, 15, 30, 45, 60, 75, 90 \omega_z^{-1}$

vious equation. The initial configuration is the ground-state structure shown in Fig.(3). The time evolution after the trap is suddenly released is shown in the sequence of snapshots of Fig.(8).

The main feature in Fig.(8) is the radial inward shrinkage of the initial state and the expansion along the polarization axis, driven by the energy gain associated by elon-

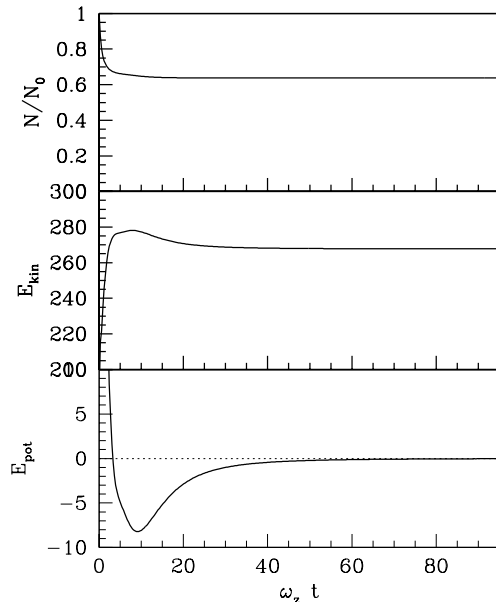


FIG. 9: Upper panel: number of atoms in the expanding condensate as a function of time. Middle and lower panel: kinetic and potential energy as a function of time.

gated configurations, and resulting in an inversion of the initial aspect ratio. In spite of the elongation towards a prolate geometry the condensate is not collapsing because of the kinetic energy associated with the expansion. A similar inversion of the aspect ratio has been observed[1] during the expansion of harmonically trapped gases when a repulsive short-range interaction was present in addition to the dipole-dipole interaction. Here, however, we find a notable dynamical stabilization of a cigar-shaped condensate (at least during the expansion time) occurring for a *purely dipolar* BEC, which would be otherwise unstable.

In Fig.(9) we show the number of atoms in the condensate during the expansion (panel (a)). The initial sudden loss is due to the sudden inward shrinkage of the cloud in the radial direction. In panel (b) and (c) we show how the kinetic energy and the dipole-dipole interaction energy vary during the expansion. The potential energy, that is initially positive due to the mainly repulsive character of the dipole-dipole interaction in the initially oblate condensate, becomes rapidly negative, signalling the predominance of aligned dipole configurations as the shape changes from oblate to prolate, but then smoothly decreases without sign of collapse.

We have verified, by comparing the above results with the expansion of the same system but with the dipole-dipole interaction turned off, that the elongation is not simply a consequence of the tighter confinement along the z -direction and the associated increased quantum pres-

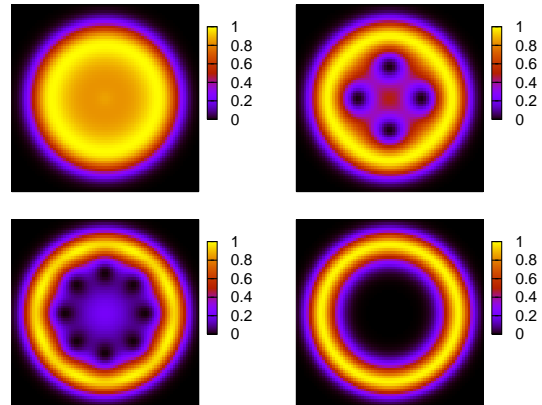


FIG. 10: (color online) Vortex structure for the condensate obtained with $D = 50$ and $\lambda = 0.11$, for four different values of the rotational frequency Ω . From left to right, and from top to bottom: $\Omega = 0.033, 0.049, 0.066, 0.082 \omega_z$

sure, but it is indeed energetically driven by the dipole-dipole attraction: when such interaction is not present, the expansion occurs in a more isotropic way.

To investigate the emergence of vortex structures in our system, we search for the lowest-energy stationary states solution of the time-dependent GP equation in a rotating frame-of-reference with constant angular velocity Ω :

$$i\hbar \frac{\partial \Psi(\mathbf{r}, t)}{\partial t} = [\hat{H} - \Omega L_z] \Psi(\mathbf{r}, t) \quad (23)$$

where L_z is the z -component of the orbital angular momentum operator.

We show in Fig.(10) our results for different values of Ω . Below a critical value $\Omega \sim 0.04 \omega_z$ the condensate cloud is not affected by the rotation. As soon as this critical angular velocity is exceeded, multiple vortex structures develop in the inner portion of the condensate where the density is lower, whose number increases with the angular velocity. Eventually, they merge into a giant vortex which empties the inner region of the trap, leading to a ring-shaped condensate.

Giant multi-quantized vortex states are known to be a feature of rotating BEC in the presence of anharmonic trap potentials [38], since anharmonic confinement improves the stability of the system against centrifugal destabilization, thus allowing to reach higher values of the angular velocity of rotation than those allowed by harmonic confinement.

IV. CONCLUSIONS

Within a mean-field approach, we have theoretically studied static and dynamical properties of a purely dipo-

lar, completely polarized pancake-shaped Bose Einstein condensate subject to highly anharmonic ("flat") confinement in the plane perpendicular to the dipole polarization axis.

Marked radial density inhomogeneities are the distinguishing features of this system, which generalize the "blood cell" cloud shapes observed in harmonically confined dipolar BECs [9, 15]. We computed the stability diagram, showing that such radially structured clouds appear in a wide variety of the parameters (dipole interaction strength and trap aspect ratio) and thus should be experimentally observable. The calculation of the excitation spectrum allows us to determine the type and symmetry of the soft modes responsible for the collapse of the system, which occurs in the form of "angular" roton excitations.

The free expansion of the dipolar gas is also studied, showing a temporary stabilization, during the expansion process, of a prolate cloud which would be unstable and

thus not be observable under stationary conditions in a purely dipolar BEC.

Finally, the rotation of the trap is studied, and the ensuing formation of multiple vortex structures. Eventually, for sufficiently high angular velocities (which would not be reachable in harmonic traps) a giant vortex develops with a wide empty core, and the BEC acquires a ring-shaped geometry.

Since highly anharmonic traps can be realized with current state-of-the-art laser optical techniques, we expect that most of the features described here will soon be confirmed by experiments.

Acknowledgments

We acknowledge useful discussions with Luca Salasnich and Maurizio Rossi.

-
- [1] J.Stuhler, A.Griesmaier, T.Koch, M.Fattori, T.Pfau, S.Giovanazzi, P.Pedri and L.Santos, Phys. Rev. Lett. **95**, 150406 (2005).
 - [2] J.D.Weinstein, R.DeCarvalho, T.Guillet, B.Friedrich, J.M.Doyle, Nature **395**, 148 (1998); H.L.Bethlem, G.Berden and G.Meijer, Phys. Rev. Lett. **83**, 1558 (1999).
 - [3] T.Lahaye et al., Rep. Prog. Phys. **72**, 126402 (2009).
 - [4] M.A.Baranov, M.Dalmonte, G.Pupillo and P.Zoller, Chem. Rev. **112**, 5012 (2012).
 - [5] J.Werner, A.Griesmaier, S.Hensler, J.Stuhler, T.Pfau, A.Simoni and E.Tiesinga, Phys. Rev. Lett.**94**, 183201 (2005).
 - [6] L.Santos, G.V. Shlyapnikov, P.Zoller and M.Lewenstein, Phys. Rev. Lett.**85**, 1791 (2000).
 - [7] S.Yi and L.You, Phys. Rev. A **63**, 053607 (2001); S.Yi and L.You, Phys. Rev. A **66**, 013607 (2002).
 - [8] D.H.J. O'Dell, S.Giovanazzi and C.Eberlein, Phys. Rev. Lett. **92**, 250401 (2004).
 - [9] S.Ronen, D.C.E. Bortolotti and J.L. Bohn, Phys. Rev. Lett. **98**, 030406 (2007).
 - [10] I.Tikhonenkov, B.A. Malomed, and A. Vardi, Phys. Rev. Lett. **100**, 090406 (2008).
 - [11] L.Santos, G.V. Shlyapnikov and M.Lewenstein, Phys. Rev. Lett.**90**, 250403 (2003).
 - [12] C.Josserand, Y.Pomeau and S.Rica, Phys. Rev. Lett. **98**, 195301 (2007).
 - [13] S.Komineas and N.R.Cooper, Phys. Rev. A **75**, 023623 (2007).
 - [14] T.Koch, T.Lahaye, J.Metz, B.Frohlich, A. Griesmaier and T.Pfau, Nature Phys. **4**, 218 (2008).
 - [15] O.Dutta and P.Meystre, Phys. Rev. A **75**, 053604 (2007).
 - [16] R.M.Wilson, S.Ronen, J.L.Bohn, Phys. Rev. A **80**, 023614 (2009).
 - [17] R.M.Wilson, S.Ronen, J.L.Bohn and H.Pu, Phys. Rev. Lett. **100**, 245302 (2008).
 - [18] S.Yi and H.Pu, Phys. Rev. A **73**, 061602(R) (2006).
 - [19] D.H.J.O'Dell and C.Eberlein, Phys. Rev. A **75**, 013604 (2007).
 - [20] M.Abad, M.Guilleumas, R.Mayol, M.Pi and D.M.Jezek, Phys. Rev. A **79**, 063622 (2009).
 - [21] R.M.W. van Bijnen, D.H.J. O'Dell, N.G.Parker and A.M.Martin, Phys. Rev. Lett. **98**, 150401 (2007).
 - [22] R.M.W. van Bijnen, A.J. Dow, D.H.J. O'Dell, N.G. Parker and A.M. Martin, Phys. Rev. A **80**, 033617 (2009).
 - [23] F. Malet, T. Kristensen, S.M. Reimann and G.M. Kavoulakis, Phys. Rev. A **83**, 033628 (2011).
 - [24] M.Abad, M.Guilleumas, R.Mayol, M.Pi and D.M.Jezek, Phys. Rev. A **81**, 043619 (2010).
 - [25] T.Lahaye, J.Metz, B.Frohlich, T.Koch, M.Meister, A.Griesmaier, T.Pfau, H.Saito, Y.Kawaguchi and M.Ueda, Phys. Rev. Lett. **101**, 080401 (2008).
 - [26] N.G. Parker, C.Ticknor, A.M. Martin and D.H.J. O'Dell, Phys. Rev. A **79**, 013617 (2009).
 - [27] J.Metz, T.Lahaye, B.Frohlich, A.Griesmaier, T.Pfau, H.Saito, Y.Kawaguchi and M.Ueda, New J. Phys. **11**, 055032 (2009).
 - [28] S.K. Adhikari, J. Phys. B: At. Mol. Opt. Phys. **46**, 115301 (2013).
 - [29] S.Ronen, D.C.E.Bortolotti, D.Blume and J.L.Bohn, Phys. Rev. A **74**, 033611 (2006).
 - [30] D.C.E.Bortolotti, S.Ronen, J.L.Bohn and D.Blume, Phys. Rev. Lett. **97**, 160402 (2006).
 - [31] A.Jaouadi, N.Gaaloul, B.Viaris de Lesegno, M.Telmini, L.Pruvost and E.Charron, Phys. Rev. A **82**, 023613 (2010).
 - [32] A.L.Gaunt, T.F. Schmidutz, I. Gotlibovych, R.P.Smith and Z. Hadzibabic, Phys. Rev. Lett. **110**, 200406 (2013).
 - [33] S.Ronen, D.C.E. Bortolotti and J.L. Bohn, Phys. Rev. A **74**, 013623 (2006).
 - [34] M.Pi, F.Ancilotto, E.Lipparini and R. Mayol, Physica E, **24**, 297 (2004).
 - [35] F.Ancilotto, M.Rossi and F.Toigo, Phys. Rev. A **88**, 033618 (2013).
 - [36] M.Nooijen and R.J.Bartlett, J. Chem. Phys. **106**, 6449 (1997).
 - [37] *Mathematical Methods for Digital Computers*, Ed.by

- A.Ralston and H.S.Wilf, vol. 1, p. 117 (Wiley, New York, 1960)
- [38] E.Lundh and A.Cetoli, Phys. Rev. A **80**, 023610 (2009).